Available online at www.sciencedirect.com
ScienceDirect
Tectonophysics 424 (2006) 223–243
TECTONOPHYSICS
www.elsevier.com/locate/tecto

Aftershocks series monitoring of the September 18, 2004 $M=4.6$ earthquake at the western Pyrenees: A case of reservoir-triggered seismicity?

M. Ruiz [a,*], O. Gaspà [a], J. Gallart [a], J. Díaz [a], J.A. Pulgar [b], J. García-Sansegundo [b], C. López-Fernández [b], J.M. González-Cortina [b]

[a] *Department of Geofísica i Tectònica, Institut de Ciències de la Terra 'Jaume Almera'- IJA-CSIC, Lluís Solé i Sabaris s/n. 08028 Barcelona, Spain*
[b] *Department Geología. Universidad de Oviedo, Arias de Velasco s/n 33005 Oviedo, Spain*

Received 21 July 2005; received in revised form 4 November 2005; accepted 25 March 2006
Available online 5 June 2006

Abstract

On September 18, 2004, a 4.6 mbLg earthquake was widely felt in the region around Pamplona, at the western Pyrenees. Preliminary locations reported an epicenter less than 20 km ESE of Pamplona and close to the Itoiz reservoir, which started impounding in January 2004. The area apparently lacks of significant seismic activity in recent times. After the main shock, which was preceded by series of foreshocks reaching magnitudes of 3.3 mbLg, a dense temporal network of 13 seismic stations was deployed there to monitor the aftershocks series and to constrain the hypocentral pattern. Aftershock determinations obtained with a double-difference algorithm define a narrow epicentral zone of less than 10 km^2, ESE–WNW oriented. The events are mainly concentrated between 3 and 9 km depth. Focal solutions were computed for the main event and 12 aftershocks including the highest secondary one of 3.8 mbLg. They show mainly normal faulting with some strike-slip component and one of the nodal planes oriented NW–SE and dipping to the NE. Cross-correlation techniques applied to detect and associate events with similar waveforms, provided up to 33 families relating the 67% of the 326 relocated aftershocks. Families show event clusters grouped by periods and migrating from NW to SE. Interestingly, the narrow epicentral zone inferred here is located less than 4 km away from the 111-m high Itoiz dam. These hypocentral results, and the correlation observed between fluctuations of the reservoir water level and the seismic activity, favour the explanation of this foreshock–aftershock series as a rapid response case of reservoir-triggered seismicity, burst by the first impoundment of the Itoiz reservoir. The region is folded and affected by shallow dipping thrusts, and the Itoiz reservoir is located on the hangingwall of a low angle southward verging thrust, which might be a case sensible to water level fluctuations. However, continued seismic monitoring in the coming years is mandatory in this area to infer more reliable seismotectonic and hazard assessments.

Keywords: Western Pyrenees; Portable array; Seismicity; Triggered earthquakes; Artificial water reservoirs; Clustering analysis

1. Introduction

On September 18, 2004, a 4.6 mbLg (magnitude derived from surface waves amplitude) earthquake

* Corresponding author. Tel.: +34 93 409 54 10; fax: +34 93 411 00 12.
E-mail address: mruiz@ija.csic.es (M. Ruiz).

0040-1951/$ - see front matter © 2006 Elsevier B.V. All rights reserved.
doi:10.1016/j.tecto.2006.03.037

occurred in the western Pyrenees, at around 20 km ESE from Pamplona city (Fig. 1). The main event was preceded by 10 foreshocks starting on September 16, two of them with magnitudes 3.3 and 3.1, and was followed by an aftershock series of up to 200 events until end of 2004, with a maximum magnitude of 3.8, as reported by the Spanish Geographical Institute (IGN) permanent seismic network (Fig. 2). In this period, people's alarm has increased considering that up to seven events of magnitudes greater than 3.0 have been felt by the population. EMS intensity values of V were reported for the main event by IGN near the epicentral zone, and it was felt with intensity IV at Pamplona and II at San Sebastian and Zaragoza, 60 km to the northwest and 150 km to the southeast, respectively (Fig. 3).

The epicentral area is characterized by two interesting facts. Firstly, the seismicity records show that there seems to be no significant seismic activity at recent times eastward of Pamplona (Fig. 2) and, secondly, it is located at around 4-km distance from the 111-m high Itoiz dam, which starts impounding in January 2004. Therefore, we decided to study in detail the aftershock series by deploying a temporary seismic network in this area, in order to get precisely the seismotectonic pattern and to evaluate whether this

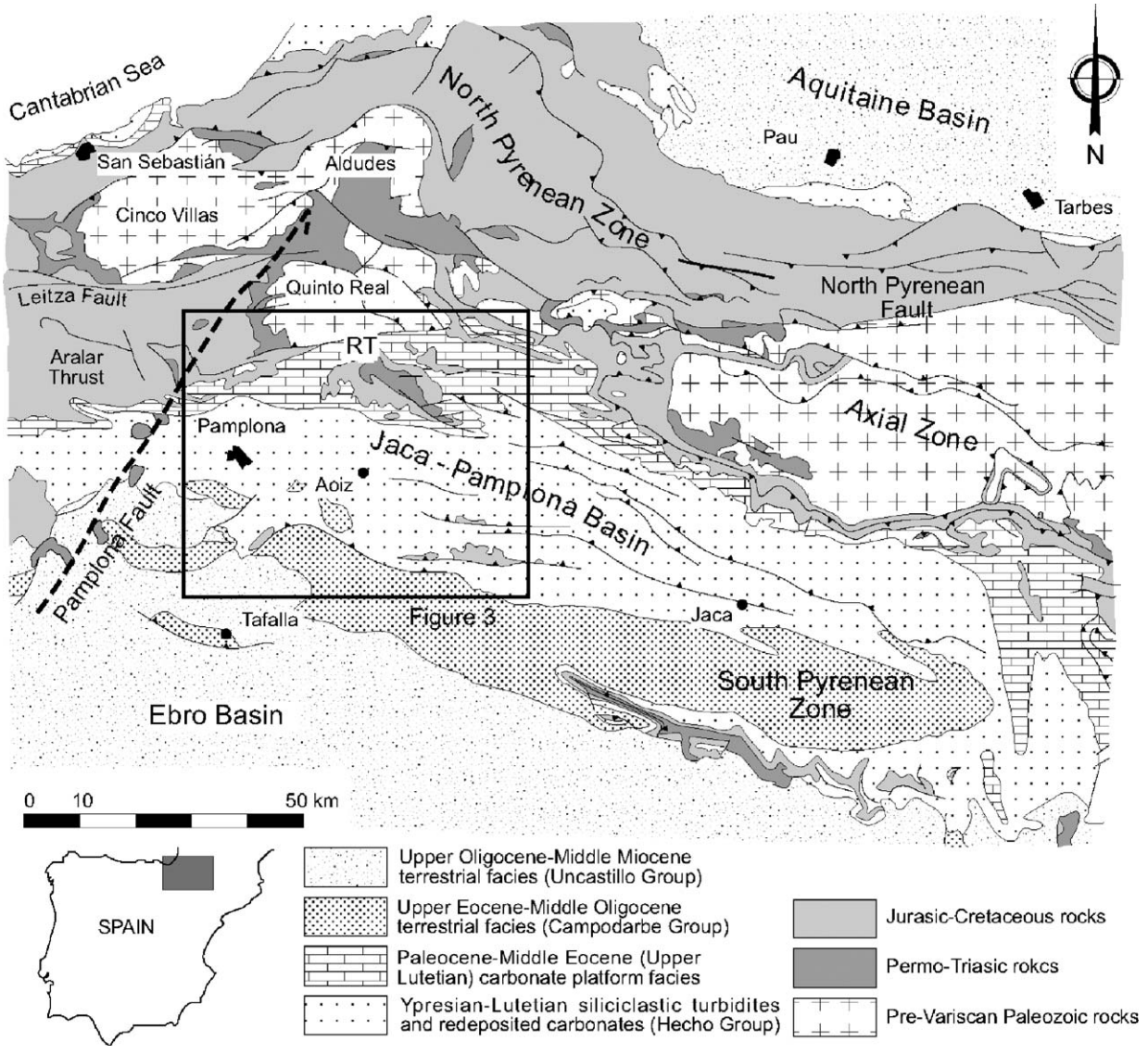

Fig. 1. Structural scheme of the study area. RT: Roncesvalles Thrust.

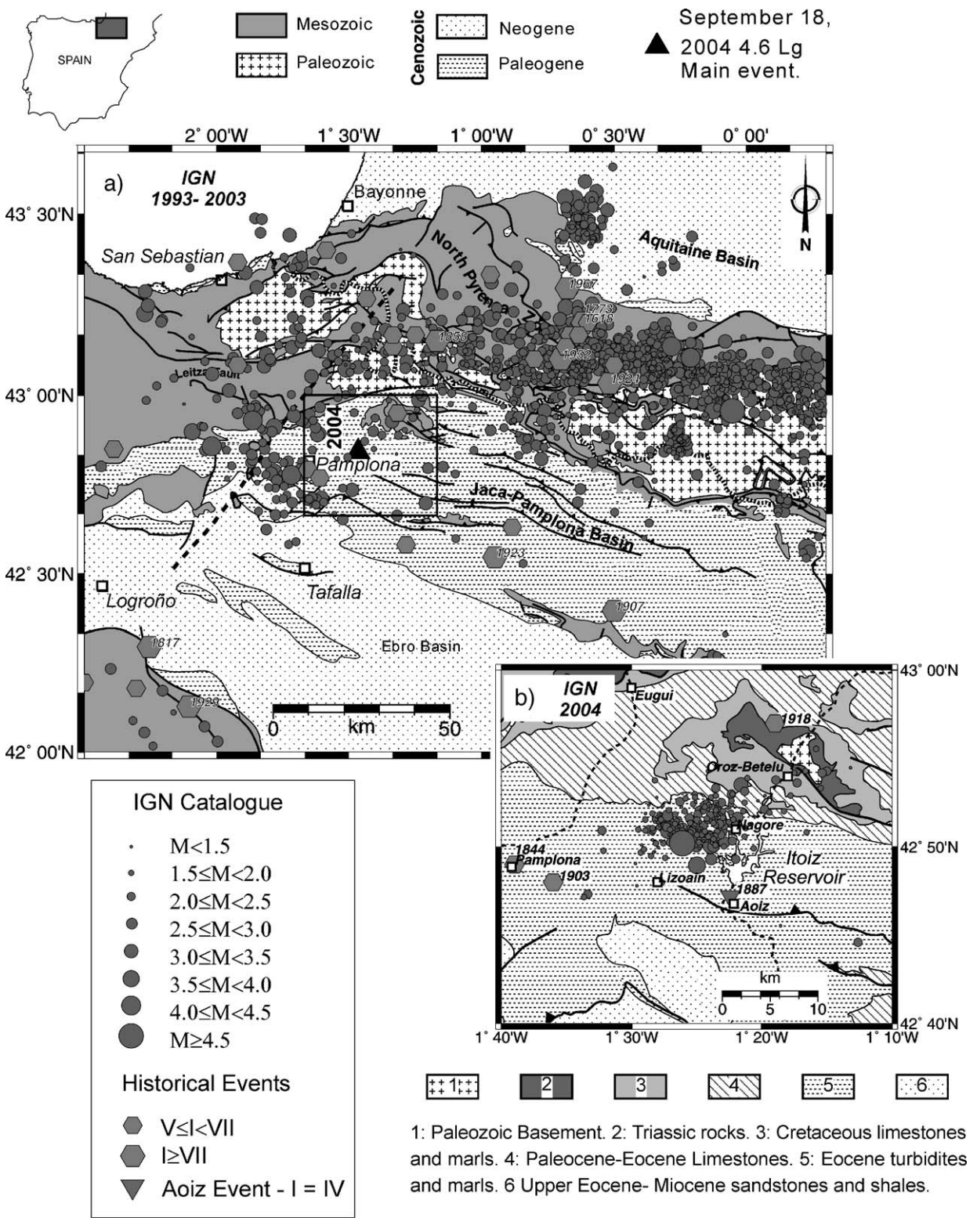

Fig. 2. (a) Epicentral location of the historical earthquakes and the events recorded by the IGN network in the western Pyrenees from 1993 to 2003. (b) Blow up of the study area; events recorded by the IGN network in the Pamplona area during 2004. The historical earthquakes are also shown.

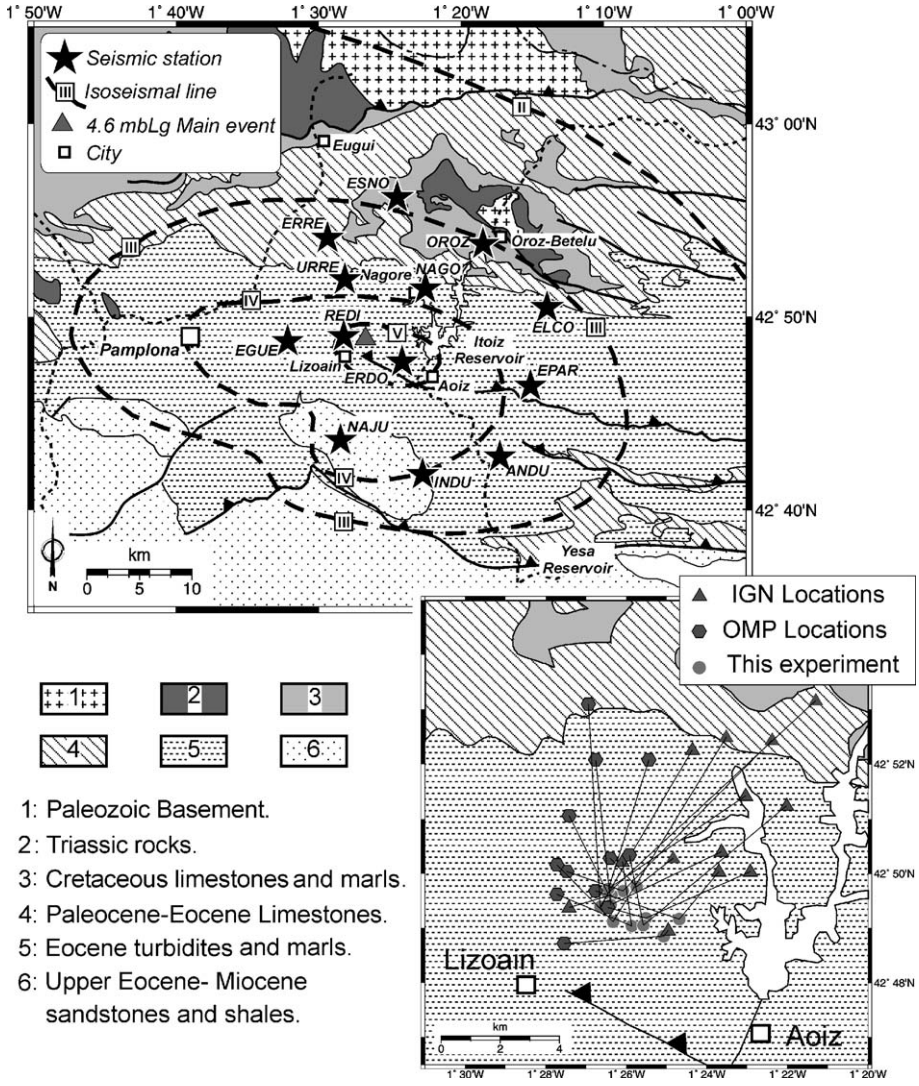

Fig. 3. (a) Location of the seismic stations used in this study. The epicenter and isoseistes of the September 18, 2004 main event are also shown. EMS intensity values of V were reported in the Lizoain village for the IGN service. (b) Epicentral determinations of some aftershocks reported by the IGN (triangles) and OMP (hexagons) services and their relocations using data from permanent and temporary networks (circles).

could be a case of reservoir-triggered seismicity (RTS).

2. Geological and seismotectonic settings

The study area (Fig. 1) is located in a region with a complex thin-skinned structure belonging to the South Pyrenean Zone (SPZ) (Cámara and Klimowitz, 1985; Muñoz et al., 1986; Turner, 1996; Teixell, 1998; Larrasoaña et al., 2003b). The SPZ constitutes the external part of the Pyrenean belt and is a Tertiary unit overriding to the south the Ebro foreland basin. This unit is north-bounded by the Paleozoic Axial Zone (PAZ), which crops out here as a series of individual massifs, known as the Paleozoic Basque Massifs (Cinco Villas and Quinto Real Massifs in Fig. 1). Between the PAZ and the North Pyrenean Zone–a Mesozoic unit overthrusting the Aquitaine foreland basin to the north–is located the North Pyrenean Fault, a major tectonic suture running east–west along the Pyrenean range and interpreted as the superficial expression of the Iberian and European plate boundaries (Choukroune, 1992). Paleomagnetic data (Van der Voo and Boessenkool, 1973; Larrasoaña et al., 2003a), seismic profiles (Gallart et al., 1981) and seismicity studies (Ruiz et al., 2006) suggested that the structural boundary associated to the NPF is prolonged westward through the Basque-Cantabrian basin along the Leiza Fault.

Another relevant structure in the area is the Pamplona Fault (PF) that runs NNE–SSW from the Ebro basin to the Paleozoic Basque Massifs (Fig. 1). It has been interpreted as a deep transverse structure separating two different structural zones, the SPZ to the east, where the most important structures verge mainly south, and the Basque-Cantabrian basin to the west, with a thicker lower Cretaceous sequence and where most structures have northward vergence (Engeser and Schwentke, 1986; Rat, 1988; Martínez-Torres, 1989; Turner, 1996; Faci et al., 1997). This structure behaved as an extensional transfer fault during the Mesozoic extensional period that leads to the opening of the Gulf of Biscay and the individualization of the Iberian Peninsula as a subplate. The PF was subsequently involved in the Tertiary compression responsible of the Pyrenean belt uplift (Larrasoaña et al., 2003b; Pedreira et al., 2003).

The epicentral region is a Mesozoic and Tertiary cover area, located in the NE of the Pamplona basin, and composed by anticlines and synclines with the axes trending to the east, but truncated at some places by E–W to ESE–WNW fault systems (Puigdefabregas et al., 1978; García-Sansegundo, 1993).

The present-day seismicity at the western Pyrenees, as reported form permanent networks (Fig. 2a), is rather moderate and mainly concentrated on the French side, that holds events with magnitudes up to 5.5 in the last decades (Gagnepain et al., 1980; Gagnepain-Beyneix et al., 1982; Gallart et al., 1985; Souriau and Pauchet, 1998; Souriau et al., 2001; Ruiz et al., 2006). This activity follows an E–W oriented strip 150 km long, 5 to 15 km wide, starting at the western edge of the NPF, at a longitude of 0.1°W (Souriau and Pauchet, 1998; Souriau et al., 2001), and continuing through the Paleozoic Basque Massifs (PBM) along the Leiza Fault (Ruiz et al., 2006). Historical seismicity appears also concentrated in the border region, along the PAZ and the PBM. Six destructive events with intensity greater than VII (Fig. 2a) are reported in this area in the recent past (Mezcua and Martínez-Solares, 1983; Martínez-Solares and Mezcua, 2003; Souriau et al., 2001).

Instrumental catalogues of the westernmost Pyrenean edge show a sparse and moderate to low magnitude activity, mainly concentrated westward of Pamplona (Fig. 2a), where events are related to the central segment of the Pamplona Fault (Grandjean et al., 1994; Souriau and Pauchet, 1998; Ruiz et al., 2006) and to the Aralar thrust (Ruiz et al., in press). An E–W seismicity belt is also found related to the Roncesvalles thrust that separates the Paleozoic Aldudes massif from the Pamplona basin (Ruiz et al., 2006). The catalogues report also a few events related to the E–W thrust systems delineating the contact between Pamplona and Ebro basins (Olivera and Gallart, 1987; Ruiz et al., 2006).

Inside the study area, four events are reported by the historical catalogue (Fig. 2b). The most important one occurred on 1903 near Pamplona city with an EMS intensity of VI. Two events with intensity V occurred near Pamplona city and the Roncesvalles thrust on 1844 and 1918, respectively, and on 1887 an event with intensity IV is reported in the Aoiz village, near the September 18, 2004 epicentral zone (Mezcua and Martínez-Solares, 1983; Martínez-Solares and Mezcua, 2003).

Close to the epicentral area is located the 111-m high Itoiz dam (Fig. 2b). The Itoiz reservoir has a maximum capacity of 418 hm^3 (cubic hectometers: 1 $hm^3 = 10^6$ m^3) and, once filled, it will cover a maximum surface of 510 km^2, aimed at irrigation and electrical power generation. During September 2004, the reservoir was only 15% filled, after starting impounding in January. A basic goal of this work is the investigation of the potential relationship between the seismic crisis and the Itoiz impounding.

3. Reservoir-triggered seismicity (RTS) setting

Triggering of earthquakes by filling of artificial water reservoirs is known for over six decades. Even if this happens at only a small percentage of reservoirs in the world, up to 90 sites have been globally identified where earthquakes have been triggered by filling of water reservoirs (Gupta, 1992; Talwani, 1997; Gupta, 2002). Four destructive earthquakes exceeding magnitude 6 took place in the 1960s in China, Zambia–Zimbabwe border, Greece and India (Rothé, 1970; Simpson, 1976; Gupta, 1992; Talwani, 1995; Chen and Talwani, 1998; Gupta, 2002; Pandey and Chadha, 2003).

The RTS usually appears under special conditions and is controlled by factors as the geology of the region, fracture location and directions, appropriate ambient stress field conditions, hydromechanical properties of the rocks, as well as the size of the reservoir, and specially the water depth, or the periodicity and extent of the water level fluctuations (Simpson, 1976; Gupta, 1992; Talwani, 1997; Gupta, 2002; Nascimento et al., 2004). It is generally agreed that the maximum possible triggered earthquake cannot exceed the maximum possible natural earthquake in the region (Gupta, 1992); this is consistent with the assumptions that near-critical pre-existing stresses are necessary in the area for the occurrence of RTS, and that the stress

produced by reservoir loading is only superimposed as a perturbation to the regional stress field (Simpson, 1976; Assumpçao et al., 2002; Rastogi, 2003). In most cases, seismicity follows either impoundment, large or rapid water-level changes, or increases of the water level that goes beyond the highest water level achieved until then (Gupta et al., 1972; Simpson and Negmatullaev, 1981; Gupta, 1983; Simpson et al., 1988; Talwani, 1997). In contrast to the natural earthquake sequences, showing the typical aftershock series, the RTS sequences present a characteristic foreshock–aftershock pattern denoting a non-uniform applied stress (Gupta, 1992; Rastogi, 2003).

Three main types of RTS (rapid, delayed or continued seismicity) are distinguished (Simpson et al., 1988; Gupta, 1992; Talwani, 1997; Gupta, 2002). The rapid response occurs when the seismicity increases immediately after the first filling of the reservoir, or following a rapid change in the water level. It is characterized by low magnitude and shallow earthquakes, occurring directly beneath or at the immediate vicinity of the reservoir. They are related to changes in elastic stress and related local pore pressure variations, and do not depend much on diffusion of water from the reservoir. In contrast, in the delayed response, the main seismic activity occurs relatively late in the life of the reservoir, some years after it has been filled and the water level maintained at a stable height. The earthquakes tend to be larger and are located at greater depths and distances larger than 10 km. Some times the reservoirs have undergone a number of apparently similar cycles of water-level changes before the dominant event occurs. This response is largely dependent on diffusion of water and pore pressure from the reservoir into the hypocentral zone. The continued response occurs when the triggered seismicity goes on at a given reservoir site, year after year or after a gap of time, depending upon the state of stress of the region and fluctuations of the water depth in the reservoir. Many reservoirs show combinations of two or three of these responses during their life.

Two RTS cases where reported in Spain by the Simpson (1976) and Gupta (1992, 2002) reviews: Canyelles (eastern Pyrenees) in 1962 and Camarillas (SE Spain) in 1964. More recently, a new case was detected in 1999 at the Tous reservoir, SE Spain (Torcal et al., 2005). In these three cases, the activity started between 1 and 4 years after the initial impounding, and presented a main event of magnitude ranging from 3.8 to 4.7. The most important earthquake, with a magnitude of 4.7, took place in the Canyelles reservoir vicinity (Rothé, 1970; Simpson, 1976).

4. Data acquisition and processing

A dense temporary network composed of 13 stations was deployed in the epicentral zone from September 22 to October 21, 2004 to monitor the aftershock seismic activity (Fig. 3a). All the instruments where Leas-Hathor digital dataloggers, working in continuous recording mode with a sampling rate of 100 sps and equipped with 1-Hz three-component seismometers. Unfortunately, several instruments started to fail after some days due to technical or environmental problems and the network coverage diminished in the last recording period.

To extract the events, a STA/LTA detection algorithm was applied to the continuous data sets. An event was retained only if it was present on three or more stations. Up to 1282 aftershock events were detected using this method. Earthquakes from the published catalogues of Spanish and French seismological services were also extracted from our continuous data set. From this set of quakes, up to 326 events had enough station coverage to be correctly located (Fig. 4).

5. Hypocentral parameters

Phase-picking and seismogram processing was done using SAC (Seismic Analysis Code) package (Goldstein and Minner, 1996; Goldstein et al., 2003). Initial hypocentral determinations were obtained from the Hypo71 code (Lee and Lahr, 1975), using a homogeneous 6 layered velocity–depth model derived from wide-angle seismic profiles across the western Pyrenees and the Basque-Cantabrian basin (Pedreira et al., 2003) (Table 1).

Up to 326 earthquakes were identified and located in this experiment. Only 70 of these events were also reported and located by Spanish and French seismological services. These events have been relocated by including the phase-picking of the portable array and

Fig. 4. (a) Epicentral location of the 326 aftershocks obtained in this study applying detection algorithms to the raw continuous data. Focal solutions obtained. Vertical cross-sections showing events distributed between 3 and 9 km depth. The horizontal and vertical error bars derived form Hypo71 inversions are shown. (b) Error body estimation for 20 selected events, approximately one event per day, obtained by making repeated locations with perturbed P- and S-phase pickings. The comparison of the Hypo71 hypocentral depths and vertical errors before and after a perturbation of the arrival times is shown. The left-hand panel shows the hypocentral depths (circles) and the 10 new depths (crosses) after a random perturbation of ±0.1 and ±0.2 s in P- and S-phases, respectively. The right-hand panel shows the corresponding depth errors.

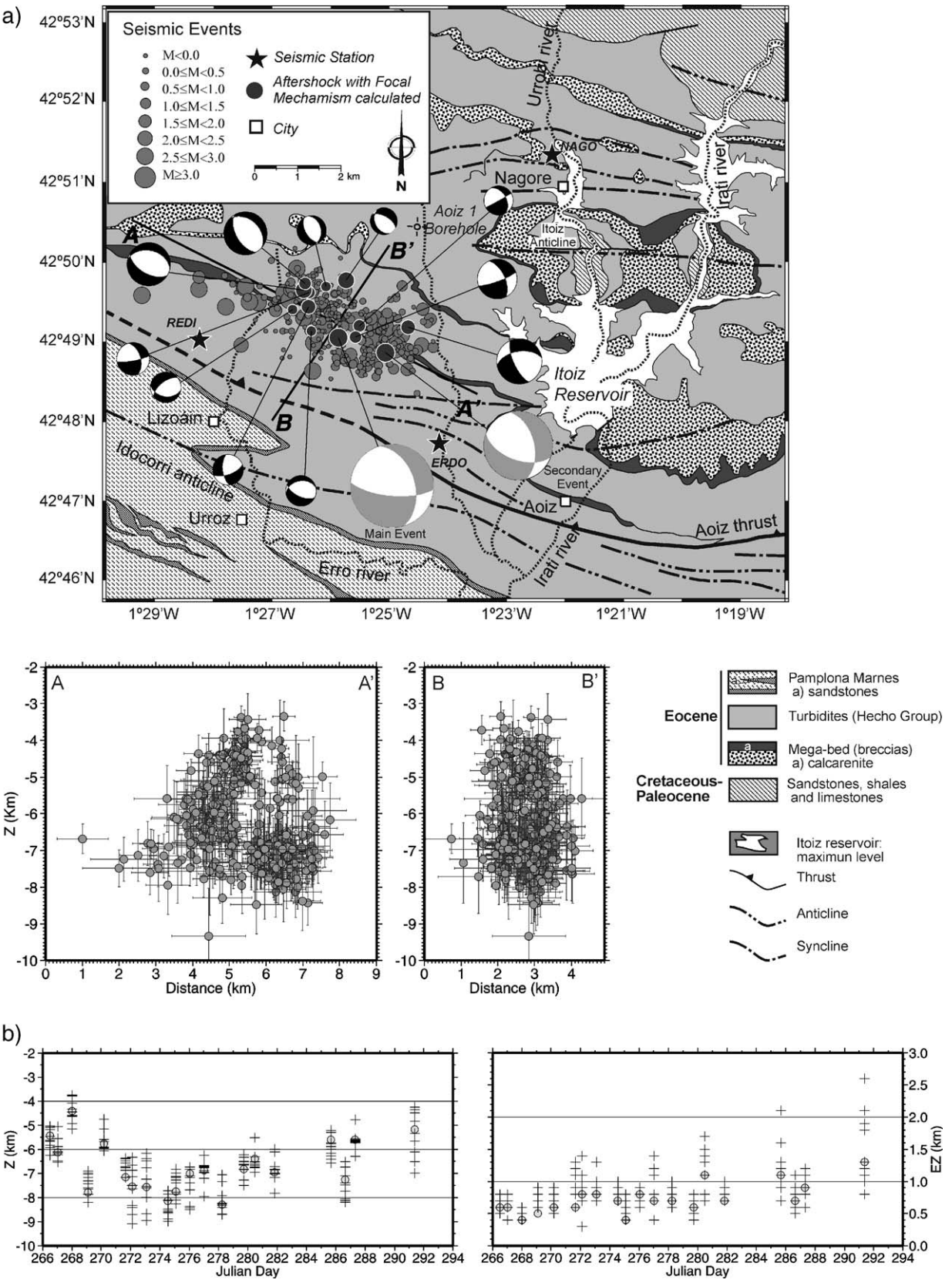
a)
Seismic Events
M<0.0
0.0≤M<0.5
0.5≤M<1.0
1.0≤M<1.5
1.5≤M<2.0
2.0≤M<2.5
2.5≤M<3.0
M≥3.0
Seismic Station
Aftershock with Focal Mechamism calculated
City
0 1 2 km
N
42°53'N
42°52'N
42°51'N
42°50'N
42°49'N
42°48'N
42°47'N
42°46'N
1°29'W
1°27'W
1°25'W
1°23'W
1°21'W
1°19'W
Urroti river
GNAGO
Nagore
Irati river
Aoiz 1 Borehole
Itoiz Anticline
A
A'
B
B'
REDI
Itoiz Reservoir
Lizoain
Idocorri anticline
ERDO
Secondary Event
Aoiz
Urroz
Main Event
Aoiz thrust
Erro river
Irati river
A
A'
B
B'
Z (Km)
Distance (km)
Eocene
Pamplona Marnes
a) sandstones
Turbidites (Hecho Group)
a
Mega-bed (breccias)
a) calcarenite
Cretaceous-Paleocene
Sandstones, shales and limestones
Itoiz reservoir: maximun level
Thrust
Anticline
Syncline
b)
Z (km)
Julian Day
EZ (km)
Julian Day

Table 1
P-velocity model used for hypocenter inversion

Z (km)	V_p (km/s)
0	5
2.2	5.6
5	6
14	6.2
22	6.7
38	8

The V_s model is obtained using a V_p/V_s ratio of 1.80.

permanent seismic networks. Those relocations clearly improved the resolution of the epicentral zone and the sparse events initially reported were grouped much closer to the main event (Fig. 3b).

Preliminary locations of the 326 earthquakes data set (Fig. 4a), obtained using the Hypo71 code, are of good quality due to the dense network coverage. The hypocenters obtained have an average RMS value of 0.08 s, being always lesser than 0.2 s. Average horizontal and vertical errors are 0.4 and 0.6 km, respectively, being always lesser than 1.7 and 2.0 km (Fig. 4). Mean value of the Gap (largest azimuthal separation between stations of the array) is approximately 120°, although the mean Gap did not exceed 80° in the first period when all stations were working and 130° when some stations started to fail at the end of the experiment, but being always lower than 180°. The aftershocks define an epicentral zone of about 14 km^2, with events distributed between 3 and 9 km depth (Fig. 4a). NW–SE and SW–NE cross-sections image a homogeneous distribution without any clear dipping structure. We tested the consistency of these results with respect to the variations of the number of stations available at each period (by decimating the full network at the beginning to the state it operated at the end, and verifying the robustness of the hypocentral locations obtained in both cases). An estimation of the error body for 20 selected events occurred all along the experiment was also obtained by making repeated locations with perturbed arrival times. Perturbations of ±0.1 and ±0.2 s considered in the P- and S-phase-picking result in little variations in the hypocentral depths and vertical errors, ensuring the stability and reliability of these preliminary locations (Fig. 4b).

Fault plane solutions of the main event and aftershocks with best azimuthal coverage (12 events with gaps less than 100° and at least 8 P-polarities, coming from temporal and permanent networks, were retained) have been computed using the FPFIT algorithm (Reasenberg and Oppenheimer, 1985) (Fig. 5). We considered the same velocity model as for the location procedure. The focal mechanism of the main event and of the M=3.8 strongest secondary event show the same solution; a normal fault with some strike-slip component, and the nodal planes oriented E–W and NNW–SSE, respectively (Figs. 4 and 5). Most of the aftershock focal mechanisms computed in this work show normal faulting with a variable component of strike-slip and differences in the azimuths of the nodal planes, although in most cases one of these planes is roughly NW–SE oriented. The accuracy of these solutions was checked by analyzing different parameters provided by the FPFIT package to assess the quality of the results. The average errors on the maximum likelihood solutions

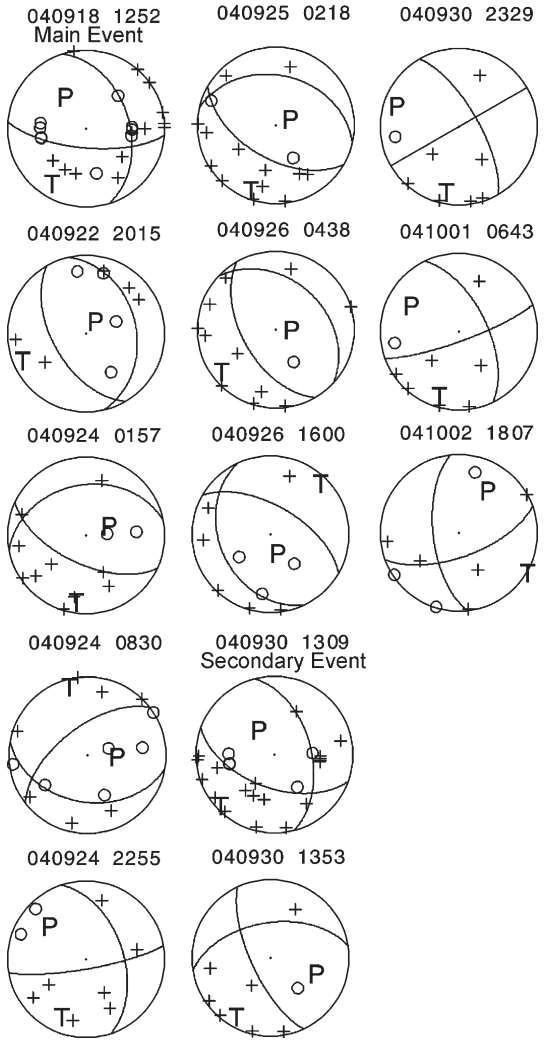

Fig. 5. Fault plane solutions (lower hemisphere equal-area projection) of the 13 studied events. For each mechanism, the date (year, month and day) and the origin time (hour and minute) are reported. P and T denote the P- and T-axes positions. Open circles and crosses indicate dilatations and compressions, respectively.

remained less than 25° for strike, dip and rake, respectively. An estimation of the misfit of the solution is provided by the F-value ($F=0$ representing a perfect fit to the data and $F=1$ a complete misfit), which is in our case lesser than 0.1. Solutions are robust for STDR (station distribution ratio) greater than 0.5 and, in our case, it is comprised between 0.52 and 0.74. Hence, the solutions obtained appear to be stable and robust, even if in some particular cases small variations in the fault plane orientations cannot be excluded. The variety of solutions obtained reveal that this seismic crisis has activated numerous small fractures, of different orientations around a general NW–SE trend, associated to a main tectonic thrust contact that presently acts as a normal fault system involving the deepening of the north-eastern block that holds the Itoiz reservoir.

6. Cluster analysis

Earthquake families, or clusters of numerous events with striking waveform similarities at individual stations, are often characteristic of aftershocks sequences (Tsujiura, 1983). The algorithm described by Maurer and Deichmann (1995), based on correlation analysis of P- and S-wave data, was applied to detect and associate events with similar waveforms. Prior to the correlation analysis, where the waveform similarity is checked station per station for P- and S-waves, a 3–15-Hz band-pass filter was applied to improve the semblance of the time series. The P-wave normalized cross-correlation matrix was obtained by correlating a time window of 1 s, starting 0.25 s before the P-phase-picked. The S-wave cross-correlation matrix resulted from the correlation of 2 s, from the N–S channel, starting 0.15 s before the S-picking. The T_S and T_P parameters of the Maurer and Deichmann (1995) algorithm, which control the S- and P-wave similarity, were set to 0.85. The cluster separation threshold (T_X) was set to 0.3 and the event association threshold (T_Y) equal to 1 (see Maurer and Deichmann, 1995 for details).

This cross-correlation method provided up to 33 families, containing at least three similar earthquakes. These earthquake families (Figs. 6 and 7) involve 218 events, 67% of the 326 analyzed aftershocks. The time–history plot in Fig. 7 shows that only 2 of the 13 focal solutions obtained belong to a same family.

The HypoDD program (Waldhauser, 2001), based on a double-difference hypocenter location approach (Waldhauser and Ellsworth, 2000), has been used to relocate the aftershock series. The double-difference technique implemented in the HypoDD program allows to use any combination of absolute travel times from earthquake catalogs and high-precision differential travel times from cross-correlation of P- and/or S-waves (Waldhauser, 2001). Therefore, the catalog data of the 326 events firstly analyzed with Hypo71 program was complemented by introducing in the HypoDD inversion the high-precision differential travel times resulting from the 218 clustered events. The DD algorithm provided a total of 288 determinations (88% of the initial data) after eliminating events with insufficient number of links to neighbors. A narrower epicentral area of less than 10 km^2 and ESE–WNW oriented is imaged (Fig. 8), delineating a clear space–time pattern, as events and families are grouped by periods and there is a geographic migration of these clusters (Figs. 7 and 8). The aftershock series started in the WNW sector of the narrow epicentral zone defined by the DD relocations. During the first 8 days, up to 16 clusters were found grouping 108 events located close to the REDI station, and distributed between 3 and 7 km depth. After the first week, a southeastward migration with an increasing hypocentral depth range was observed. The 17 remaining families were mainly located in the ESE sector, near the ERDO station, with hypocentral distributions ranging from 5 to 9 km depth (Fig. 8).

7. Statistical parameters of the aftershocks series

NAJU station (Fig. 3) recorded one of the most complete time sequence of events and this data set has been statistically analyzed; all the detections resulting from STA/LTA algorithm were extracted for this station. During the 29 days of the experiment, NAJU detected 1431 aftershocks, whereas the algorithm for the whole network resulted in 1282 events.

This data set has been used to better constrain the evolution of the seismic series, including the characterisation of the time-decrement of the seismic activity and its frequency–magnitude distributions.

7.1. Temporal evolution of the seismicity

Fig. 9a shows the temporal evolution of the seismicity as detected by the NAJU station. During the first days, from September 22 to 29 (Julian days 266 to 273), the expected aftershock exponential decrease related to the September 18 main event is not clearly imaged, as the network was not operative until 4 days after the main event. Moreover, on September 30, a magnitude 3.8 mbLg event occurred and an abrupt increment of the seismicity was detected. NAJU

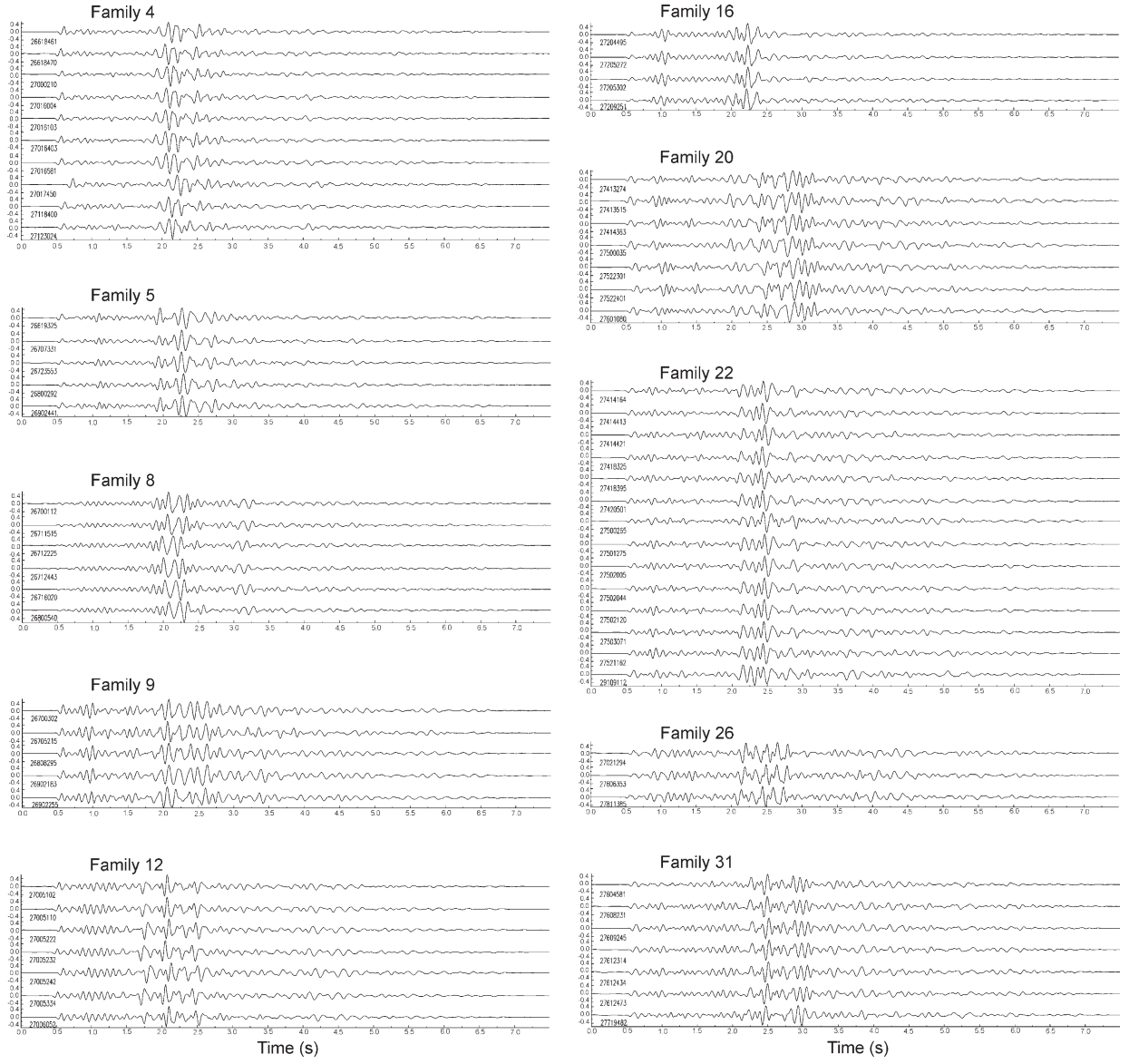

Fig. 6. Vertical component seismograms, 3–15 Hz band-pass filtered, recorded at URRE station of 10 families obtained using cross-correlation methods. A total of 33 families relating the 67% of the relocated aftershocks were obtained.

recorded up to 906 events from September 30 to October 21 (Julian days 274 to 295).

The occurrence rate of aftershocks sequences is empirically described by the modified Omori formula (Utsu et al., 1995):

$$n(t) = K(C + t)^{-p}$$

where $n(t)$ is the frequency of aftershocks per unit time (days) after the main shock. The exponent p is a rate constant for aftershocks decay and is generally found between 0.5 and 2 (Helmstetter et al., 2003), being independent on the magnitude of the main event but reflecting mechanical conditions of the crust on a regional scale (Ogata, 1999; Utsu, 2002). The offset time C is often not well constrained and may partly account for the incompleteness of catalogues close to main shocks (Hauksson and Jones, 1989). This constant is small, 1 day at most, and provides a regularization at short times preventing the event rate to reach infinity at the time of the mainshock (Ogata, 1999; Helmstetter et al., 2003). In many cases, the aftershock sequences appear complex and are better described by the Epidemic Type of Aftershock Sequences (ETAS)

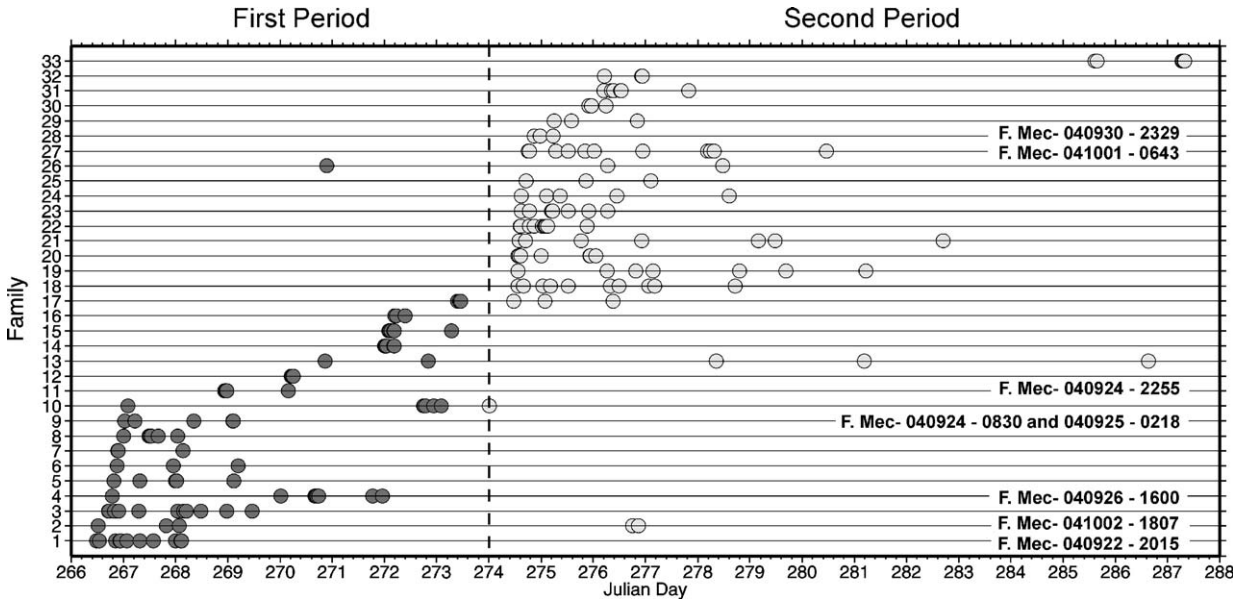

Fig. 7. Time–history plot showing the occurrence of the individual families. Two periods are imaged, first occurring during Julian days 266–273 and the second during 274–295. Focal solutions of events belonging to families are indicated.

model, which is a stochastic point process in which every event can produce its offspring events (Guo and Ogata, 1997; Ogata, 1999). In particular, the rate of aftershocks induced by an earthquake that occurred at time t_i with magnitude M_i is given by:

$$\lambda_i(t) = K(c + t - t_i)^{-p} e^{\alpha(M_i - M_o)}$$

for time $t > t_i$. The parameters K, α, c and p are constant to all the earthquakes, and M_o is the magnitude threshold of the catalogue. α is typically between 0.2 and 3.0, and measures the magnitude sensitivity of an earthquake in generating its offspring or aftershocks in a wide sense (Guo and Ogata, 1997; Ogata, 1999). The total occurrence rate is the sum of the rate of all the preceding earthquakes and a constant μ, which stands for the rate occurrence of background activity,

$$\lambda(t) = \mu + \Sigma\lambda_i(t), \text{ summing for all } t_i < t$$

The ETASX program included in the SASeis package (Utsu and Ogata, 1997) was used to obtain maximum likelihood estimates (MLE) of the ETAS model parameters. We obtained the following values using a magnitude threshold of −1:

$$\mu = 3.13,\ K = 0.59,\ c = 0.0048,\ \alpha = 0.35,\ p = 1.34$$

We have calculated the cumulative number of events predicted by the ETAS model by integration of the total occurrence rate and compared with our data, obtaining consistent results (Fig. 9b).

7.2. Local magnitudes and Gutenberg-Richter distribution

In order to fix the magnitudes of the aftershock events, we first established a local magnitude (M_L) formula, defined as an empirical relationship involving the total signal duration. We have used a relation of the form (Lee et al., 1972):

$$M_L = a + b \log T$$

where T is the total signal duration in seconds, measured from the onset of the first P-arrival to the point at which the signal falls into the background noise, averaged for all the stations to reduce the data scattering, and a and b are constants determined statistically. In our case, epicentral distances are almost constant for each station and always lower than 20 km, and we have not taken them into account in the adjust. A least-squares analysis was used to fit the coefficients of the formula. The local magnitudes of 30 events catalogued by the IGN service and recorded with a good signal-to-noise ratio were used as reference. This resulted in the following equation, with a correlation coefficient of 91%:

$$M_L = -4.1697 + 3.2884 \log T$$

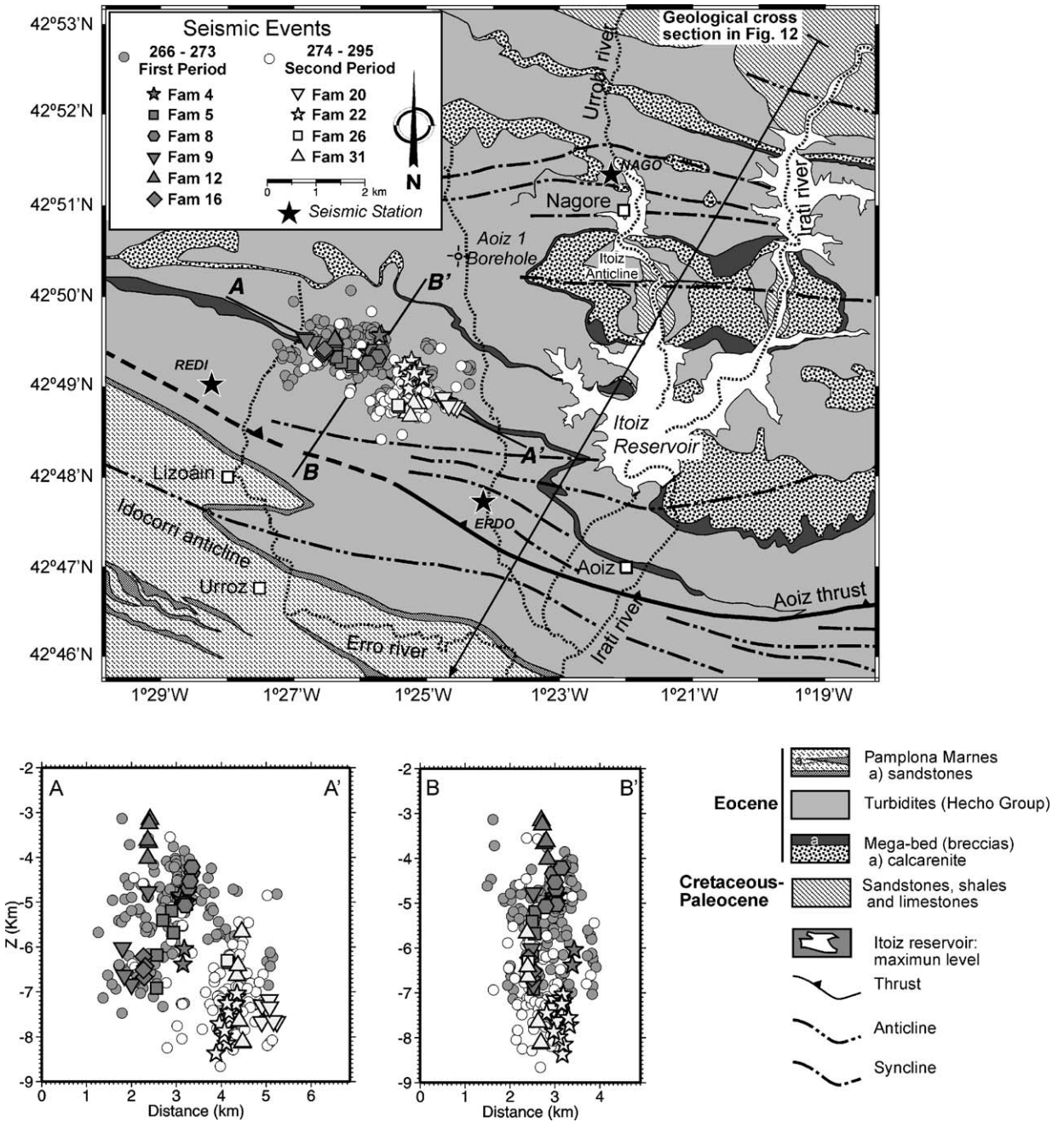

Fig. 8. Relocation of the complete catalogue after the double-difference approach, using absolute and differential travel times from cross-correlation of P- and S-waves. Lower panels show vertical cross-sections of the hypocenters. Different symbols and grey intensities are used to separate events belonging to different families and periods, indicated in the inset, and illustrate the southeastward migration of the seismicity.

The catalogue of the NAJU station was also used to obtain, after a linear regression adjustment, the *b*-value of the cumulative Gutenberg-Richter distribution:

$$\log N = a - bM$$

where N is the total number of events with magnitude greater than M. The b coefficient is normally close to 1, but it may range between 0.5 and 1.5 depending on the region (Guo and Ogata, 1997; Nanjo et al., 1998; Utsu, 1999).

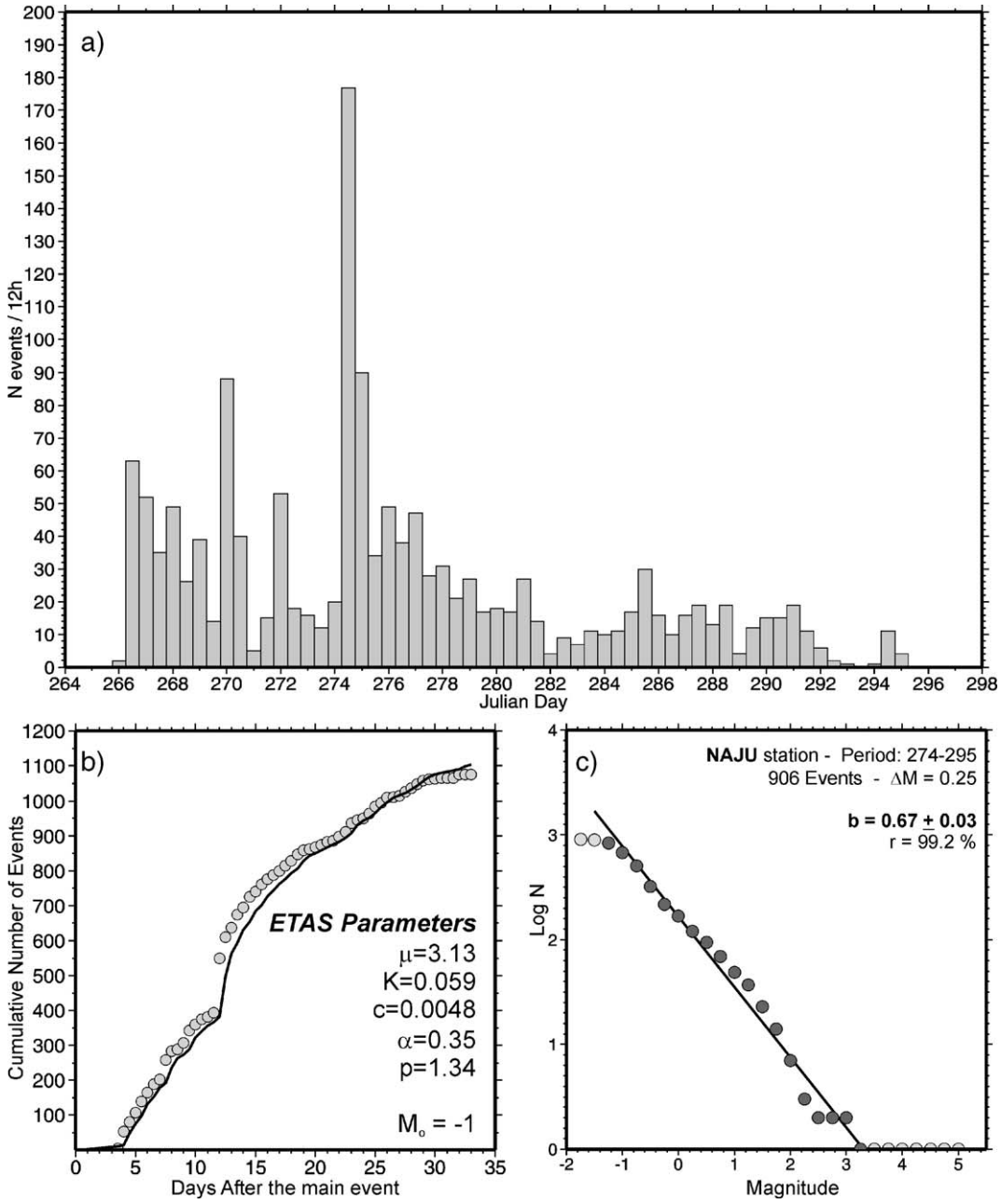

Fig. 9. (a) Frequency distribution of the 1431 events obtained by the detection algorithms applied to NAJU station. (b) Cumulative number of events every 12 h as function of time (circles) compared with that inferred from the ETAS model (bold line). (c) Cumulative Gutenberg-Richter distribution and *b*-value fitting using 0.25 magnitude increments.

A statistical analysis of the *b* slope variability was performed testing different intervals of magnitude increments, comprised between 0.1 and 0.5, and a stable solution was always obtained. A mean *b*-value of 0.67 ± 0.03 was inferred using the 906 events following the September 30 secondary event (Fig. 9c). The error bar of this calculation includes the statistical error from least-squares fitting and the *b*-value variations due to the different magnitude increments.

The *b*-value resulting from this experiment is lower than the obtained in other studies carried out near the Pamplona Fault; Njike-Kassala et al. (1992) obtained $b = 0.96 \pm 0.1$ and Ruiz et al. (in press) $b = 0.80 \pm 0.02$.

The *p* and *b* statistical parameters could be used to try to discriminate between natural and reservoir-triggered seismicity. Reservoir-associated sequences use to present higher *b*-values and slow rates of aftershock decay compared to natural-sequences (Gupta et al., 1972; Gupta, 1992, 2002; Rastogi, 2003); however, the values obtained in this study correspond to a very specific aftershock episode and they do not show the characteristic trend of the RTS series. Therefore, more data in this area from longer time periods are needed to infer relevant constraints.

8. Relationship between the water level and the seismicity

The fluctuations of the reservoir water level, provided by the Ebro Hydrological Confederation Data Centre (SAIH-CHE), have been correlated with the temporal evolution of the seismicity at the vicinity of the reservoir, using the IGN catalogue (Fig. 10). Data comprise from the first impoundment of the Itoiz reservoir, on January 2004, to October 2005. In the initial period, from January to April, the hydrological data shows that the water level increased from 0 to 70 hm^3 with rapid and abrupt volume variations. From April to mid-May 2004, the mean water level was kept approximately constant, but suffering rapid volume changes of more or less 4 hm^3 in few days. After this period, to end of August, the volume of water was maintained stable at 70 hm^3. A rapid water level change started on August 21, as the volume of the reservoir was decreased, reaching on October 15 the minimum of 56 hm^3. Then, from November 2004 to mid-March 2005, the volume was raised to 190 hm^3 and kept constant from April to mid-June 2005. At the end of this stable period, the water level was again decreased to 70 hm^3 (Fig. 10). All these water level changes are part of a set of scheduled engineering tests to check the site and dump stability.

Prior to reservoir impounding, the IGN catalogue does not show any significant activity in this area. Only an event of intensity IV appears in the historical

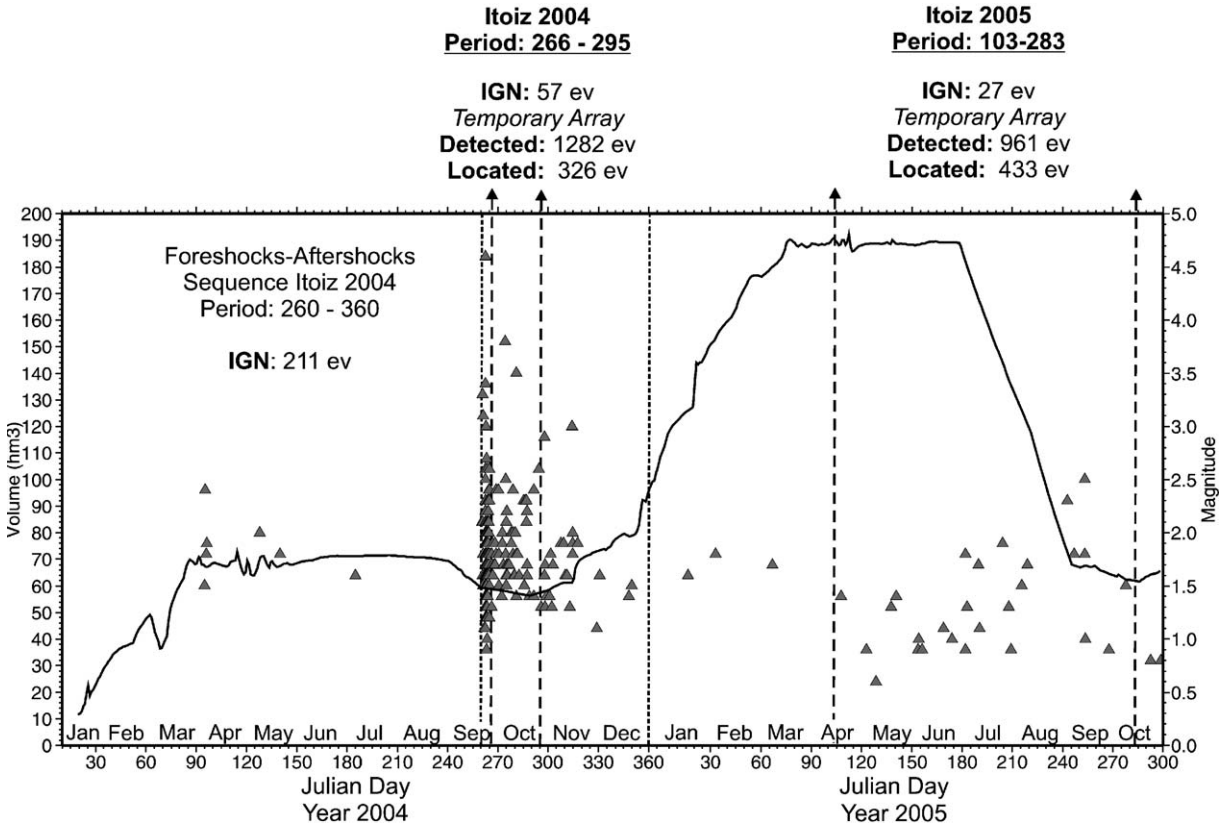

Fig. 10. Correlation of the water level (bold line) and the seismicity reported by the IGN service (triangles) in the area close to the reservoir concerning the September 2004 seismic crisis and the activity related to the 2005 scheduled engineering tests. The evolution of the water volume in time in front of the magnitude of the events occurred is shown. Number of events reported by the IGN permanent array and from our study is indicated for the different periods.

catalogue on 1887 near Aoiz village, and a few isolated and low magnitude events are reported in the precedent years. During the 1993–2003 period, only eight earthquakes of magnitudes less than 2.6 are reported in an area of 400 km^2 around the 2004 epicentral area (Fig. 2). From April to beginning of July 2004, the IGN catalogue reported seven events with magnitudes ranging from 1.5 to 2.4 in the area of the reservoir. Later on, the foreshocks–aftershocks series started on September 16, when the water level was near the summer's minimum. On mid-October, the water level was again increased, exceeding the 70 hm^3 on mid-November, when the seismic series stopped. In this period, up to 200 events with magnitudes ranging from

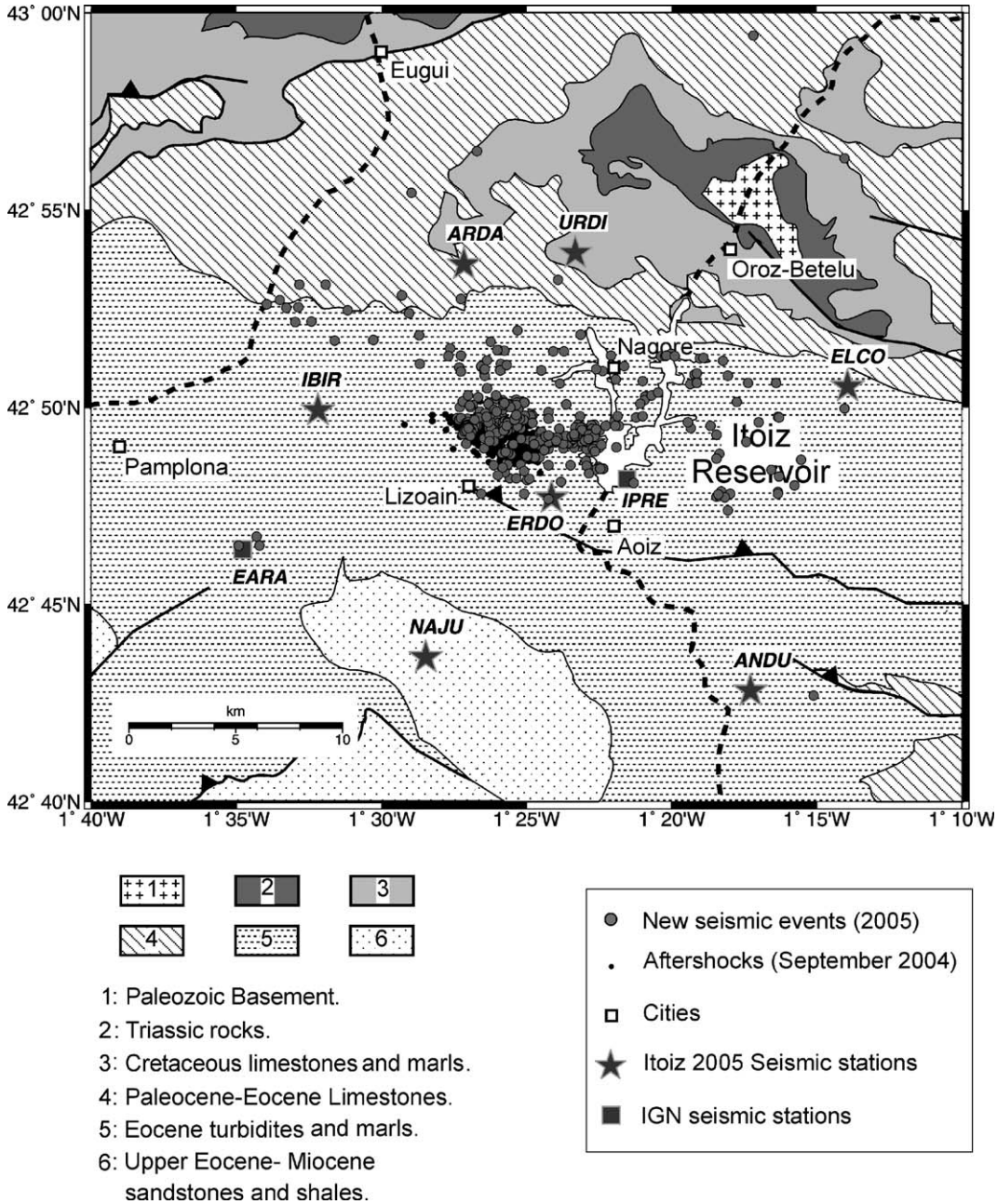

Fig. 11. Location of the seismic stations deployed during Itoiz 2005 experiment to monitor the engineering tests to check the site and damp stability. The grey circles show the epicentral locations of 433 events located during this second experimental period. The September 2004 aftershocks are also shown (small dark circles).

0.9 to 4.6 mbLg were reported by the IGN catalogue (Fig. 10), clustered in the western sector of the reservoir, and within our 1-month experiment, up to 1431 aftershocks were detected related to the main event of September 18.

When the water level was again increased, from November 2004 to mid-March 2005, the seismic activity decreased, with only three events in the first months of 2005 in the IGN catalogue, although it remained higher than the precedent years. Then, during the stable period started on April 2005 and the July rapid decrease, the seismicity seems to increase again, as 27 events were detected from April to mid-October 2005 by the permanent array (Fig. 10).

With the aim of monitoring the effect of the 2005 scheduled engineering tests of water level changes, a new portable seismic network was deployed in April 2005 (Fig. 11). It was composed of seven stations, most of them reoccupying previous emplacements, but adding also some new sites to enlarge the monitored area. To date, during the first 6 months, up to 961 new events of magnitude less than 2.5 have been detected, at a mean rate of five earthquakes per day. From this set of quakes, up to 433 events, 27 of which were events also detected by the IGN service, had enough station coverage to be correctly located. The preliminary hypocentral determinations show an enlarged epicentral zone with events propagating to the WNW and the ESE, over an area approximately 30 km long and 10 km wide (Fig. 11). The activity remains shallow, mainly located between 0 and 6 km depth. The 2004 seismic focus is still active, but the locations are now sparser and present an important core concentrated close to the western border of the Itoiz reservoir.

9. Discussion

The hypocentral results obtained in this study, showing a shallow activity highly clustered at the vicinity of the reservoir, the lack of any remarkable activity in the area prior to the impoundment of the Itoiz reservoir, and the correlation of the fluctuations of the reservoir water level with the evolution of the seismic activity during the years 2004 and 2005 (Fig. 10), all favour the explanation of this foreshock–aftershock series as a rapid response case of reservoir-triggered seismicity, burst by the first impoundment of the Itoiz reservoir. The rapid water level change occurred between end of August and beginning of September, after a stable period, might be at the origin of the September 18, 2004 series, the seismic activity continuing at an unusual high level during the engineering tests of 2005.

Rapid response, or Initial seismicity is the most widely observed category of RTS. Most case histories where appropriate data are available can be explained by the response to initial loading, rapid water volume changes, or loading at a later time above the highest water level achieved (Simpson and Negmatullaev, 1981; Talwani, 1997). They are related to changes in elastic stress and related pore pressure changes, and do not depend on diffusion of water from the reservoir into the hypocentral zone. Usually, there is a decrease of activity with time, the seismicity returning to the pre-impoundment levels.

The stress changes due to reservoir impounding are governed by the Coulomb criterion: the increase of pore pressure, or decrease in the coefficient of friction and cohesion results in weakening the rocks and leading them to failure (Talwani, 1997). Roeloffs (1988) pointed out that reservoir load induced stresses at seismogenic depths that are very small (<0.1 MPa) and can only disturb the ambient tectonic stress field. However, some studies have shown that stress changes as low as 0.01 MPa are sufficient to induce failure in critically stressed fault zones (Reasenberg and Simpson, 1992; Harris, 1998; Árnadóttir et al., 2003). Therefore, the reservoir impounding creates stresses which are superimposed on a pre-existing tectonic stress regime and, in areas of moderate strain accumulation (regions of low natural seismicity or areas adjacent to major seismic regions), the stress changes from the reservoir may be significant compared to rates of stress change from natural processes and the effects on seismicity will be more obvious than in an area of high strain accumulation (Simpson, 1976). The September 2004 foreshock–aftershock sequence with a 4.6 mbLg main event could be the consequence of a small perturbation produced by the first impounding of the Itoiz reservoir in a critically stressed fault zone. The fact that some earthquakes of comparable size could have happened in the study area in historic times may even favour the RTS hypothesis. It would indicate that the region has been placed to near-critical stress field several times, producing earthquakes of similar magnitude in the past, and now the Itoiz reservoir might have acted as a trigger of the accumulated stress field.

Fig. 10 shows that the September 2004 seismic crisis could be triggered by the summer's water level decrease after a stable period and it was finished when the water level was again increased. Then, during the 2005 spring–summer engineering tests, the seismicity seems to start again after a stable period and an abrupt water

level descend. A similar pattern has been observed in other RTS cases, where correlations between abrupt decreases or changes of water level and a considerable increase of the seismicity are reported (e.g.: Simpson and Negmatullaev, 1981; Assumpçao et al., 2002; Gupta, 2002; Hassoup, 2002; Pandey and Chadha, 2003; Torcal et al., 2005). Nevertheless, some cases of continuous seismicity related to cyclic water level variations, which present its maximum activity approximately following the water level descent, can also be explained by a time delay between maximum water level and the subsequent increase in seismic activity, as the dominant mechanism for triggering events in continuous cases of RTS is largely dependent on diffusion of water and pore pressure (Roeloffs, 1988; Talwani, 1995; Gupta et al., 1997; Pandey and Chadha, 2003; Nascimento et al., 2004; Nascimento et al., 2005). The Itoiz reservoir impoundment is much too recent, and it has never been submitted to complete cycles of the water level variations, to be able to conclude if it is only a rapid response case of RTS, which will disappear in the next future, or, on the contrary, it will continue undergoing cyclic seismic episodes. A long-time history of hydraulic and seismic data is also required to establish hydraulic parameters, as time lags between variations of the water level and seismicity. The space–time pattern observed in the 2004 seismic crisis, which took place in a short period of a month, is reflecting the seismic activation of different minor fractures associated to the main thrust and could also be considered a case of pore pressure diffusion due to stress redistribution caused by the main shock or as reciprocal stress triggering of individual aftershocks. It cannot be attributed to fluid diffusion through the rock mass as this involves a long time delay and cluster migration takes place during years (e.g.: Simpson and Negmatullaev, 1981; Chen and Talwani, 1998; Nascimento et al., 2004, 2005). Nevertheless, new data obtained in the 2005 experiment, showing an enlarged epicentral zone covering a wide area around the reservoir, could be indicating that fluid movements cannot be excluded, and the diffusive processes altering the pore pressure in the seismogenic region could be starting to play an important role after some time of the reservoir impoundment.

Complex geologic structure undoubtedly plays an important role in the mechanics of RTS, but the effect of the type of faulting and the location of the reservoir with respect to it is the most important factor controlling the RTS (Simpson, 1976; Roeloffs, 1988; Talwani, 1997). Roeloffs (1988) found that, for a reservoir subjected to cyclic water level fluctuations, earthquakes tended to

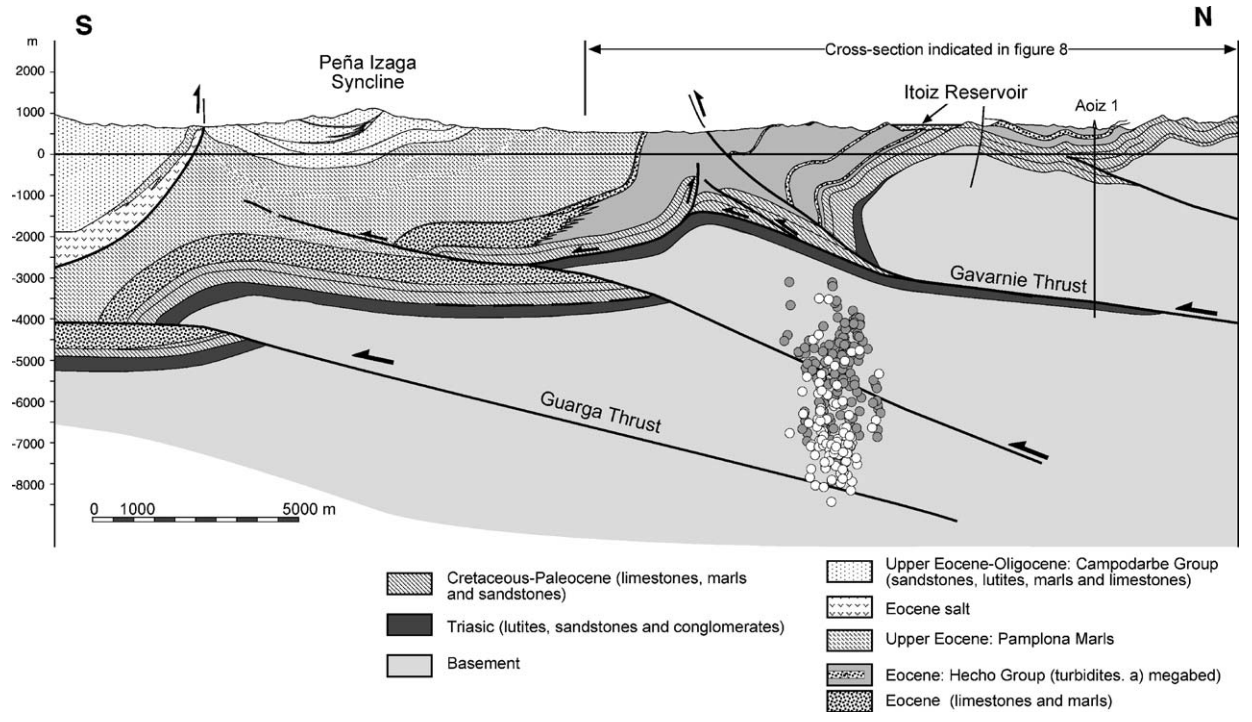

Fig. 12. Geological cross-section, approximately in a SW–NE direction, with the 2004 aftershocks hypocenters superimposed showing the location of the reservoir respect to the regional faulting.

occur below the reservoir if it was located over a vertical strike-slip fault, on a steeply dipping normal fault, or on the hanging wall of a shallowly dipping thrust. On the other hand, if it was located on the footwall of a steeply dipping reverse fault, the activity occurred on the side where the fault dips away from the reservoir. The Itoiz reservoir is located in a complex thin-skinned region, affected by shallow dipping thrusts. Specifically, it is located on the hanging wall of a low angle southward verging thrust associated to Gavarnie thrust system (Fig. 12). Therefore, this might be a case sensible to the water level fluctuations and deserves further seismic monitoring. Smooth filling/emptying of reservoirs appears to be the key to reduce the hazard of RTS, but the threshold rate of loading/unloading, to avoid occurrence of strong earthquakes, would vary from one site to another (Simpson, 1976; Simpson and Negmatullaev, 1981; Gupta, 1983).

The focal solutions obtained in this study showing normal faulting with some differences in the strike-slip component are mechanisms usually found in the western Pyrenees. On the Quaternary and the present time, the active structures in Iberia appear to be mainly strike-slip and normal faults, as during the Pliocene most of thrust faults became inactive (Herraiz et al., 2000; Jabaloy et al., 2002). The maximum stress direction in this region is NNW–SSE to NW–SE as is observed in most of the P-axes orientation (Nicolas et al., 1990; Delouis et al., 1993, Grandjean et al., 1994; Souriau et al., 2001). However, the dips of the P-axes range from subhorizontal to subvertical; thus, cases of reverse faulting are also present (Souriau et al., 2001). Most of the focal mechanisms obtained in this work also show the P-axes oriented in the NW–SE direction. The different orientations of the strike around the general NW–SE trend, producing the variety of normal solutions obtained, are indicating that different minor fractures associated to the main Gavarnie thrust have been activated in this seismic crisis. Its present activity as a normal fault, deepening the northeastern block where the Itoiz reservoir is located, evidences crustal readjustments after the shutting down of the Pyrenean orogenic activity. This fact has also been observed in other western Pyrenees structures, as in the Leiza Fault (Ruiz et al., 2006).

10. Conclusions

The deployment, after the September 18, 2004 earthquake, of a dense temporal seismic network, composed by 13 stations within epicentral distances lower than 20 km, has provided an accurate image of the seismic series occurred in an area that apparently lacked of seismotectonic relevance. The epicentral zone is located in a folded area affected by shallow dipping thrusts, belonging to the South Pyrenean Zone, but the seismic catalogues of Pyrenean networks doesn't show any remarkable activity in the area prior to the September 4.6 mbLg earthquake.

The main shock, which was widely felt in the region, was preceded by series of foreshocks, starting 2 days before the main event, and followed during a month with almost 1400 aftershocks. Six of these earthquakes had magnitudes higher than 3.0 and were also felt in the area, especially a 3.8 mbLg secondary event, increasing the alarm of the population.

Aftershock determinations, obtained with a double-difference algorithm and using cross-correlation data, define a narrow epicentral zone less than 10 km^2, ESE–WNW oriented, with the events distributed between 3 and 9 km depth. Cross-correlation techniques were applied to detect and associate events with similar waveforms. The 33 families obtained, relating the 67% of the relocated aftershocks, show a relevant space–time distribution. Events are grouped per periods and the clusters migrate in space from WNW to ESE slightly increasing the hypocentral depth.

Up to 12 aftershock focal solutions were computed showing normal faulting with a variable component of strike-slip, with the most consistent nodal plane oriented NW–SE and dipping to the NE.

The geographical location of the epicentral zone, located not far from the 111-m high Itoiz dam, the shallow hypocentral distribution of the aftershocks, and the correlation between the seismicity and the fluctuations of the reservoir water level, favour the explanation of this seismic activity as a rapid response case of RTS, burst by the first impounding of the Itoiz reservoir on January 2004.

The deployment, starting on April 2005, of a new seismic network composed by seven stations, has shown that the area still remains active. The epicentral zone, as depicted from the preliminary location of 433 new events, is now sparser. Although an important cluster of events appears concentrated on the western border of the Itoiz reservoir, the epicenters extend mainly in the E–W direction and cover with shallow activity an area of 300 km^2 around the reservoir.

The present-day seismicity pattern, significantly higher than the one reported in the last decades, provides further support to the RTS explanation. However, to be able to conclude if it is a rapid response case of RTS that will disappear in the future, or, on the contrary, it will continue undergoing cyclic seismic episodes related to cyclic water level variations, a

longer-time history of hydraulic and seismic data is required.

The results obtained enhance the importance of using dense temporal networks to infer relevant hazard constraints related to water reservoir impoundment. However, continued seismic monitoring for the coming years is mandatory in this area to infer more reliable seismotectonic and hazard assessments.

Acknowledgements

This work was carried out with the support of the MARCONI (REN2001-1734) project from the Spanish MCYT. M.R. benefited from a PhD grant from the Spanish MCYT. We would like to thank to the responsible of the IGN, RENASS, OMP, CEA and CHE databases for sharing the seismic and hydrological data used in this study. We acknowledge Dr. A. Villaseñor for his inestimable suggestions and comments. The authors also wish to thank Dr. Tomas Fischer and an anonymous reviewer for their constructive comments on this manuscript.

References

Árnadóttir, T., Jónsson, S., Pedersen, R., Gudmundsson, G.B., 2003. Coulomb stress changes in South Iceland seismic zone due to two large earthquakes in June 2000. Geophys Res Lett 30 (5), 1205, doi:10.1029/2002GL016495.

Assumpçao, M., Marza, V., Chimpliganond, L., Soares, C., Carvalho, J.E., Caixeta, J., Amorim, D., Cabral, A., 2002. Reservoir-induced seismicity in Brazil. Pure Appl Geophys 159, 597–617.

Cámara, P., Klimowitz, J., 1985. Interpretación geodinámica de la vertiente centro-occidental surpirenaica (cuencas de Jaca-Tremp). Estud Geol (Madrid) 41, 391–404.

Chen, L., Talwani, P., 1998. Reservoir induced seismicity in China. Pure Appl Geophys 153, 133–149.

Choukroune, P., 1992. Tectonic evolution of the Pyrenees. Annu Rev Earth Planet Sci 20, 143–158.

Delouis, B., Haessler, H., Cisternas, A., Rivera, L., 1993. Stress tensor determination in France and neighbouring regions. Tectonophysics 221, 413–437.

Engeser, T., Schwentke, W., 1986. Towards a new concept of the tectogenesis of the Pyrenees. Tectonophysics 129, 233–242.

Faci E., Castiella J., Del Valle J., García A., Díaz A., Salvany J.M., Cabra P., Ramírez del Pozo J., Meléndez A., 1997. Mapa geológico de Navarra, Escala 1:200.000. Gobierno de Navarra, Spain 142 pp.

Gagnepain, J., Mediano, T., Cisternas, A., Ruegg, J.C., Vadell, M., Hatzfeld, D., Mezcua, J., 1980. Sismicité de la région d'Arette (Pyrénées-Atlantiques) et mécanismes au foyer. Ann Geofis 36, 499–508.

Gagnepain-Beyneix, J., Haessler, H., Modiano, T., 1982. The Pyrenean Earthquake of February 29, 1980: an example of complex faulting. Tectonophysics 85, 273–290.

Gallart, J., Banda, E., Daignières, M., 1981. Crustal structure of the Paleozoic Axial Zone of the Pyrenees and transition to the North Pyrenean Zone. Ann Geophys 37 (3), 457–480.

Gallart, J., Daignières, M., Gagnepain-Beyneix, J., Hirn, A., 1985. Relationship between deep structure and seismicity in the western Pyrenees. Ann Geophys 3 (2), 239–248.

García-Sansegundo J. Memoria y mapas geológicos a escala 1: 25.000 de la hoja n° 142 (Aoiz), cuadrantes de Aoiz (I), Irurozqui (II), Monreal (III) y Domeño (IV). Diputación Foral de Navarra; 1993.

Goldstein, P., Dodge, D., Firpo, M., Minner, L., 2003. SAC2000: signal processing and analysis tools for seismologists and engineers. In: Lee, W.H.K., Kanamori, H., Jennings, P.C., Kisslinger, C. (Eds.), Invited contribution to "The IASPEI International Handbook of Earthquake and Engineering Seismology", vol. 81B. Academic Press, London.

Goldstein, P., Minner, L., 1996. SAC2000: seismic signal processing and analysis tools for the 21st century. Seismol Res Lett 67, 39.

Grandjean G, Daignières M, Gallart J, Hirn A, Répartition de la sismicité dans la partie occidentale des Pyrénées. C.R. Acad. Sci. Paris, 1994; t. 319, série II, P. 527–533.

Guo, Z., Ogata, Y., 1997. Statistical relations between the parameters of aftershocks in time, space and magnitude. J Geophys Res 102 (B2), 2857–2873.

Gupta, H.K., 1983. Induced seismicity hazard migration through water level manipulation at Koyna, India: a suggestion. Bull Seismol Soc Am 73 (2), 679–682.

Gupta, H.K., 1992. Reservoir-induced earthquakes. Elsevier, Amsterdam. 364 pp.

Gupta, H.K., 2002. A review of recent studies of triggered earthquakes by artificial water reservoirs with especial emphasis in Koyna, India. Earth-Sci Rev 58, 279–310.

Gupta, H.K., Rastogi, B.K., Narain, H., 1972. Common features of the reservoir-associated seismic activities. Bull Seismol Soc Am 62 (2), 481–492.

Gupta, H.K., Rastogi, B.K., Chadha, R.K., Mandal, P., Sarma, C.S.P., 1997. Enhanced reservoir-induced earthquakes in Koyna region, India, during 1993–95. J Seimol 1, 47–53.

Harris, R.A., 1998. Introduction to special section: stress triggers, stress shadows, and implications for seismic hazard. J Geophys Res 103 (B10), 24347–24358.

Hassoup, A., 2002. Seismicity and water level variations in the Lake Aswan area in Egypt 1982–1997. J Seimol 6, 459–467.

Hauksson, E., Jones, L.M., 1989. The 1987 Whittier narrows earthquake sequence in Los Angeles, southern California: seismological and tectonic analysis. J Geophys Res 94 (B7), 9569–9589.

Helmstetter, A., Ouillon, G., Sornette, D., 2003. Are aftershocks of large Californian earthquakes diffusing? J Geophys Res 108 (B10), 2483. doi:10.1029/2003JB002503.

Herraiz, M., De Vicente, G., Lindo-Ñaupari, R., Giner, J., Simón, J.I., González-Casado, J.M., Vadillo, O., Rodríguez-Pascua, M.A., Cicuéndez, J.I., Casas, A., Cabañas, L., Rincón, P., Cortés, A.L., Ramírez, M., Lucini, M., 2000. The recent (upper Miocene to Quaternary) and present tectonic stress distributions in the Iberian Peninsula. Tectonics 19, 762–786.

Jabaloy, A., Galindo-Zaldívar, J., González-Lodeiro, F., 2002. Palaeostress evolution of the Iberian Peninsula (late Carboniferous to present-day). Tectonophysics 357, 159–186.

Larrasoaña, J.C., Parés, J.M., Del Valle, J., Millán, H., 2003a. Triassic paleomagnetism from the western Pyrenees revisited: implications for the Iberian–Eurasian Mesozoic plate boundary. Tectonophysics 362, 161–182.

Larrasoaña, J.C., Parés, J.M., Millán, H., Del Valle, J., Pueyo, E.L., 2003b. Paleomagnetic, structural, and stratigraphic constraints on

transverse fault kinematics during basin inversion: the Pamplona Fault (Pyrenees, north Spain). Tectonics 22 (6), 1071. doi:10.1029/2002TC001446.

Lee, W.H.K., Bennet, R.E., Meagher, K.L., 1972. A method of estimating magnitude of local earthquakes from signal duration. . U.S. Geol. Surv. Open File Report 1–28.

Lee, W.H.K., Lahr, J.C., 1975. HYPO71 (revised): a computer program for determining hypocenters, magnitudes and first motion pattern of local earthquakes. U.S. Geol. Surv. Open File Report 75–311.

Martínez-Solares J.M., Mezcua J., 2003. Catálogo sísmico de la península Ibérica (880 ac–1900). Instituto Geográfico Nacional. Monografía N. 18 254 pp.

Martínez-Torres L.M., 1989. El Manto de los Mármoles (Pirineo Occidental): geología estructural y evolución geodinámica. PhD thesis. Univ. País Vasco, Spain. 294 pp.

Maurer, H., Deichmann, N., 1995. Microearthquake cluster detection on waveform similarities, with an application to the western Swiss Alps. Geophys J Int 123, 588–600.

Mezcua J., Martínez-Solares J.M., 1983 Simicidad en el área Ibero-Magrebí. Publicación. N. 203. Instituto Geográfico Nacional, 302 pp.

Muñoz, J.A., Martínez, A., Vergés, J., 1986. Thrust sequence in the Spanish eastern Pyrenees. J Struct Geol 8 (3–4), 399–405.

Nanjo, K., Nagama, H., Sotomura, M., 1998. Rates of aftershock decay and the fractal structure of active fault systems. Tectonophysics 287, 173–186.

Nascimento, A.F., Cowie, P.A., Lunn, R.J., Pearce, R.G., 2004. Spatio-temporal evolution of induced seismicity at Açu reservoir, NE Brasil. Geophys J Int 158, 1041–1052.

Nascimento, A.F., Lunn, R., Cowie, P.A., 2005. Modelling the heterogeneous hydraulic properties of faults using constraints from reservoir-induced seismicity. J Geophys Res 110, B09201. doi:10.1029/2004JB003398.

Nicolas, M., Santoire, J.P., Delpech, P.Y., 1990. Intraplate seismicity: new seismotectonic data in western Europe. Tectonophysics 179, 27–53.

Njike-Kassala, J.D., Souriau, A., Gagnepain-Beyneix, J., Martel, L., Vadell, M., 1992. Frequency–magnitude relationship and Poisson's ratio in the Pyrenees, in relation to earthquake distribution. Tectonophysics 215, 363–369.

Ogata, Y., 1999. Seismicity analysis through point-process modeling: a review. Pure Appl Geophys 155, 471–507.

Olivera, C., Gallart, J., 1987. Sismicidad de la región de Navarra (Pirineos Occidentales). Rev Geofís. 43, 221–234.

Pandey, A.P., Chadha, R.K., 2003. Surface loading and triggered earthquakes in Koyna-Warma region, western India. Phys Earth Planet Inter 139, 207–223.

Pedreira, D., Pulgar, J.A., Gallart, J., Díaz, J., 2003. Seismic evidence of Alpine crustal thickening and wedging from the western Pyrenees to the Cantabrian mountains (North Iberia). J Geophys Res 108 (B4), 2204. doi:10.1029/2001JB001667.

Puigdefabregas C, Rojas B, Sánchez Carpintero I, Valle de Lerchundi J., 1978. Memoria y Mapa Geológico de España, E. 1:50.000, 2ª ser., Hoja n° 142 (Aoiz). Inst. Geol. Min. Esp.

Rastogi B.K., 2003. Studies on Koyna and other reservoir induced earthquakes. Proceedings of the Workshop on Current Practices and Future Trends in Earthquake Geotechnical Engineering, Bangalore, 23–24 December, 8 pp.

Rat, P., 1988. The Basque-Cantabrian basin between the Iberian and European plates; some facts but still many problems. Rev Soc Geol Esp 1 (3–4), 327–348.

Reasenberg, P.A., Oppenheimer, D., 1985. FPFIT, FPPLOT and FPPAGE: Fortran computer programs for calculating and displaying fault-plane solutions. U.S. Geol. Surv. Open File Report 85–739. 25 pp.

Reasenberg, P.A., Simpson, D.W., 1992. Response of regional seismicity to the static stress changes produced by Loma Prieta earthquake. Science 255, 1687–1690.

Roeloffs, E.A., 1988. Fault stability changes induced beneath a reservoir with cyclic variations in water level. J Geophys Res 93 (B3), 2107–2124.

Rothé, J.P., 1970. Seismes Artificiels. Tectonophysics 9, 215–238.

Ruiz, M., Gallart, J., Díaz, J., Olivera, C., Pedreira, D., López, C., González-Cortina, J.M., Pulgar, J.A., 2006. Seismic activity at the Western Pyrenean edge. Tectonophysics 412 (3–4), 217–235. doi:10.1016/j.tecto.2005.10.034.

Ruiz, M., Díaz, J., Gallart, J., Pulgar, J.A., González-Cortina, J.M., López, C., in press. Seismotectonic constraints at the western edge of the Pyrenees: aftershock series monitoring of the 2002 February 21, 4.1 Lg earthquake. Geophys J Int.

Simpson, D.W., 1976. Seismicity changes associated with reservoir loading. Eng Geol 10, 123–150.

Simpson, D.W., Negmatullaev, S.K., 1981. Induced seismicity at Nurek reservoir, Tadjikistan, USSR. Bull Seismol Soc Am 71 (5), 1561–1586.

Simpson, D.W., Leith, W.S., Scholz, C.H., 1988. Two types of reservoir-induced seismicity. Bull Seismol Soc Am 78 (6), 2025–2040.

Souriau, A., Pauchet, H., 1998. A new synthesis of Pyrenean seismicity and its tectonic implications. Tectonophysics 290, 221–244.

Souriau, A., Sylvander, M., Rigo, A., Fels, J.F., Douchain, J.M., Ponsolles, C., 2001. Sismotectonique des Pyrénées: principales constraintes sismologiques. Bull Soc Géol Fr 172 (n 1), 25–39.

Talwani, P., 1995. Speculation on the causes of continuing seismicity near Koyna reservoir, India. Pure Appl Geophys 145 (1), 167–174.

Talwani, P., 1997. On the nature of the reservoir-induced seismicity. Pure Appl Geophys 150, 473–492.

Teixell, A., 1998. Crustal structure and orogenic material budget in the west central Pyrenees. Tectonics 17 (3), 395–406.

Torcal, F., Serrano, I., Havskov, J., Utrillas, J.L., Valero, J., 2005. Induced seismicity around the Tous New Dam (Spain). Geophys J Int 160, 144–160.

Tsujiura, M., 1983. Characteristic frequencies for earthquake families and their tectonic implications: evidence from earthquake swarms in the Kanto District, Japan. Pure Appl Geophys 4, 573–600.

Turner, J.P., 1996. Switches in subduction direction and the lateral termination of mountain belts: Pyrenees–Cantabrian transition, Spain. J Geol Soc (Lond.) 153 (4), 563–571.

Utsu, T., 1999. Representation and analysis of the earthquake size distribution: a historical review and some new approaches. Pure Appl Geophys 155, 509–535.

Utsu, T., 2002. Statistical features of seismicity. In: Lee, W.H.K., Kanamori, H., Jennings, P.C., Kisslinger, C. (Eds.), Invited contribution to "The IASPEI International Handbook of Earthquake and Engineering Seismology", vol. 81A. Academic Press, London.

Utsu, T., Ogata, Y., 1997. Statistical analysis of seismicity. Algorithms for earthquake statistics and prediction. IASPEI Software Library, vol. 6. International Association of Seismology and Physics of the Earth's Interior in Collaboration with the Seismological Society of America, pp. 13–94.

Utsu, T., Ogata, Y., Matsumura, S., 1995. The centenary of the Omori Formula for a decay law of aftershocks activity. J Phys Earth 43, 1–33.

Van der Voo, R., Boessenkool, A., 1973. Permian paleomagnetic result from the western Pyrenees delineating the plate boundary between the Iberian peninsula and stable Europe. J Geophys Res 78 (23), 5118–5127.

Waldhauser, F., 2001. HypoDD—a program to compute double-difference hypocenter locations. . U.S. Geological Survey. Open File Report 01–113.

Waldhauser, F., Ellsworth, W.L., 2000. A double-difference earthquake location algorithm: method an application to the northern Hayward Fault, California. Bull Seismol Soc Am 90 (6), 1353–1368.